Available online at www.sciencedirect.com
ScienceDirect
Acta Biomaterialia 4 (2008) 976–988
Acta BIOMATERIALIA
www.elsevier.com/locate/actabiomat

Segmented poly(esterurethane urea)s from novel urea–diol chain extenders: Synthesis, characterization and in vitro biological properties

P.C. Caracciolo [a], A.A.A. de Queiroz [b], O.Z. Higa [c], F. Buffa [a], G.A. Abraham [a,*]

[a] *Instituto de Investigaciones en Ciencia y Tecnología de Materiales, INTEMA (UNMdP-CONICET), Av. Juan B. Justo 4302, B7608FDQ Mar del Plata, Argentina*

[b] *Department of Physics and Chemistry, Instituto de Ciências Exatas, Universidade Federal de Itajubá (UNIFEI), Av. BPS. 1303, 37500-903 Itajubá, Minas Gerais, Brazil*

[c] *Instituto de Pesquisas Energéticas e Nucleares-IPEN/CNEN-SP, São Paulo, Brazil*

Received 25 September 2007; received in revised form 7 December 2007; accepted 4 February 2008
Available online 2 March 2008

Abstract

This work describes the preparation, physicochemical characterization, mechanical properties and in vitro biological properties of two bioresorbable aliphatic segmented poly(esterurethane urea)s (SPEUU) based on poly(ε-caprolactone) diol (PCL diol), 1,6-hexamethylene diisocyanate and two novel urea–diol chain extenders. To strengthen the interactions through hydrogen bonding in the hard segments of SPEUU, novel chain extenders containing urea groups were synthesized and used in the SPEUU formulation. The different chemical structures of the chain extenders modulated the phase separation of soft and hard segments, as demonstrated by the thermal behavior. The hard segment association was enhanced using a diurea–diol chain extender. The biological interactions between the obtained materials and blood were studied by in vitro methods. Research on the protein adsorption, platelet adhesion and thrombus formation is presented. Studies of protein adsorption onto polymeric surfaces showed that SPEUU adsorbed more albumin than fibrinogen. Studies on platelet adhesion and thrombus formation of SPEUU-coated coverslips indicated the antithrombogenic behavior of these surfaces. The synthesized SPEUU revealed no signs of cytotoxicity to Chinese hamster ovary cells, showing satisfactory cytocompatibility.

Keywords: Segmented poly(esterurethane urea)s; Chain extender; Blood compatibility; Cytotoxicity

1. Introduction

Having been used in the medical field for almost half a century, segmented polyurethanes (SPU) remain one of the most common groups of biomaterials applied to the fabrication of implantable devices, owing to the possibility of tailoring their physical properties [1]. The development of biodegradable and biocompatible SPU and polyurethane networks with labile moieties susceptible to hydrolysis in the polymer backbone has been a subject of considerable interest in recent years [2–5]. The highly variable chemistry of SPU may be used to generate polymers that exhibit a wide range of physical and chemical properties. In this sense, a careful selection of monomers can lead to a biodegradable SPU whose properties can be tailored to many different biomedical applications. Depending on their mechanical properties, chemical composition and surface characteristics, biodegradable SPU can potentially be used in designing cardiovascular implants, drug delivery devices, non-adhesive barriers in trauma surgery, injectable augmentation materials and tissue adhesives [1,6].

Nowadays, the use of polyurethanes in tissue–organ regeneration scaffolds for replacement or repair of a wide range of biological tissues is an area of intensive research,

* Corresponding author. Tel.: +54 223 481 6600; fax: +54 223 481 0046.
E-mail address: gabraham@fi.mdp.edu.ar (G.A. Abraham).

1742-7061/$ - see front matter © 2008 Acta Materialia Inc. Published by Elsevier Ltd. All rights reserved.
doi:10.1016/j.actbio.2008.02.016

and some examples of their uses in medicine are in articular cartilage repair, cancellous bone graft substitutes, artificial skin, cardiovascular tissue engineering, meniscal reconstruction and meniscal prostheses.

The unique and versatile properties of SPU elastomers are directly related to their two-phase microstructure, with hard domains acting as thermally reversible crosslinking points, and soft domains constituting the flexible segments [7]. Polyester soft segments can be used to provide hydrolytically labile segments. When appropriately designed, chain extenders are able to impart specific properties to the material. Thus, labile groups may be introduced in the hard segments through the use of appropriate short-chain compounds [8,9], and the incorporation of urea linkages strengthens hard segment interactions through the hydrogen bonding of urea groups in adjacent chains [10].

Biomedical segmented poly(esterurethanes) (SPEU) and segmented poly(esterurethane urea)s (SPEUU) based on PCL soft segments of different chain lengths and aliphatic diisocyanates, such as 1,4-butanediisocyanate (BDI), hexamethylene diisocyanate (HDI), L-lysine ethyl (or methyl) ester diisocyanate (LDI), 1,4-*trans*-cyclohexane diisocyanate (CHDI) and isophorone diisocyanate (IPDI), have been synthesized using a broad variety of chain extenders. There are several examples of chain extenders reported in the literature, including (i) short-chain diamines: 1,4-butanediamine or putrescine (BDA) [11–14], and amino acids or amino acid derivatives such as L-lysine ethyl ester or L-ornithine ethyl ester [5,15] and L-phenylalanine-based diester [16,17]; (ii) short-chain diols: 1,4-butanediol (BDO) [14,18,19], 1,4:3,6-dianhydro D-sorbitol or isosorbide diol [20], cyclohexane dimethanol [21], ethambutol dihydrochloride [22], 1,3-propanediol [23], 3-hexine-2,5-diol [2], and triblocks of BDO-BDI-BDO [14,24]; (iii) short-chain amino-diols such as 2-amino-1-butanol [20]; (iv) sulphydryl compounds such as 2-mercaptoethyl ether [20]; and (v) short-chain diurea–diphenols based on tyramine or tyrosine [10,25]. Water was also used to create hard segments of different lengths through urea-linkage formation [26].

It is well documented in the literature that the tissue compatibility of SPU depends upon the response of cells and enzymes on the material after implantation in the biological organism. The most important factors which affect SPU biocompatibility are the protein adsorption and cellular interactions that will occur at the biomaterial–tissue interface [27]. The study of in vitro and in vivo cellular behavior at the interface of synthetic materials used for implantable devices or cell culture scaffolds is fundamental. In vitro tests such as cytotoxicity, protein adsorption and blood-cell interaction with SPU may provide findings regarding the interactions of biomedical devices in biological media in a short period of time, which would contribute to minimize animal testing.

In this work, two linear SPEUU were synthesized from poly(ε-caprolactone) diol (PCL diol), HDI and two novel aliphatic urea–diol chain extenders prepared and characterized in the authors' laboratory. The physicochemical properties of the synthesized macrodiol, chain extenders and polymers are described, and the in vitro biological properties are addressed and discussed.

2. Materials and methods

2.1. Materials

ε-caprolactone, triethylene glycol (TEG), 2-aminoethanol (AE) and HDI were obtained from Aldrich, and used as received except for TEG, which was dried under vacuum at 60 °C for 24 h prior to use. LDI was kindly donated by Kyowa Hakko Kogyo Co., Ltd, Japan. Stannous 2-ethylhexanoate (Aldrich) and dibutyltin dilaurate (Fluka) were used as catalysts. *N*,*N*-dimethylacetamide (DMAc) (Aldrich) was kept over molecular sieves (4 Å) and distilled under vacuum. Human serum albumin (HSA) and fibrinogen (HFb) were purchased from Sigma. Protein solutions were freshly prepared in 10 mM phosphate buffered saline (PBS, pH 7.4) to a concentration of 1 mg ml^{-1} before each experiment.

2.2. Synthesis of SPEUU

2.2.1. PCL diol synthesis

Linear PCL diol with number-average molecular weight (M_n) 2200 Da was synthesized by charging a pre-determined amount of ε-caprolactone into a three-necked flask containing dried TEG. Stannous 2-ethylhexanoate (0.1 wt.%) was then added, and the reaction was carried out in bulk for 24 h with magnetic stirring in a nitrogen atmosphere at 130 °C.

2.2.2. Chain extenders synthesis

Two urea–diol chain extenders were synthesized from aliphatic diisocyanates (LDI or HDI) and AE at a molar ratio of 1:2. The reactions were carried out at 0 °C with magnetic stirring and nitrogen flow. The absence of an isocyanate peak (2250–2280 cm^{-1}) in the Fourier transform infrared (FTIR) spectrum confirmed complete conversion, which yields the chain extenders AE–L–AE and AE–H–AE, respectively.

2.2.3. SPEUU synthesis

SPEUU were synthesized via a standard two-step polymerization. Briefly, PCL diol was reacted with HDI in a 1:2.01 molar ratio at 80 °C in a nitrogen atmosphere. The pre-polymerization step proceeded for 1 h with stirring in the presence of dibutyltin dilaurate (0.1 wt.% of macrodiol). The prepolymers were subsequently reacted with either AE–L–AE or AE–H–AE chain extenders for 6 h at 80 °C. The resulting slurry was precipitated over cold distilled water, washed and dried under vacuum. The samples were designated PHL and PHH, depending on the chain extender used: AE–L–AE and AE–H–AE, respectively. Films were prepared by solution casting. SPEUU were dissolved in DMAc

(10% w/v). Solutions were cast onto siliconized Petri dishes, and the solvent was evaporated at 60 °C. The 0.3-mm-thick films were dried under vacuum for 24 h.

2.3. Physicochemical characterization

The M_n of PCL diol was measured using an acetylation procedure with phthalic anhydride described in ASTM D4274-99. Three titration values were averaged. ^1H and ^{13}C nuclear magnetic resonance (NMR) spectroscopy was performed using a Bruker AM-500 NMR spectrometer operating at 500 MHz. All spectra were obtained at room temperature from 5% w/v $CDCl_3$ solutions (for PCL analysis) or DMSO-*d*6 (for chain extenders analysis), using a delay time between pulses of 5 s. Infrared analysis was performed using a Mattson Genesis II FTIR spectrometer at room temperature. Spectra of the monomers were obtained from KBr pellets. For SPEUU films, attenuated total internal reflectance (ATR-FTIR) spectra were obtained using the same spectrometer equipped with an ATR accessory. Spectra were collected from 64 scans at 2 cm^{-1} resolution. Differential scanning calorimetry (DSC) was carried out in a Shimadzu DSC-50 calorimeter. Scans were performed at a heating rate of 10 °C min^{-1}. Thermograms were obtained in the range −100 to 250 °C under nitrogen purge. The glass transition temperature was taken at the onset of the transition. The intrinsic viscosity of SPEUU samples was measured in DMAc at 30 ± 0.1 °C using an Ubbelohde Type OC viscometer (Cannon).

2.4. Mechanical properties

Uniaxial stress–strain data were obtained from an Instron model 4467 testing machine. Sample strips of $35 \times 5 \times t$ (mm^3) ($t = 0.3$–0.5 mm) were cut from polymer films. Tests were performed using a crosshead speed of 5 mm min^{-1}, an extensometer for elastomers, and a loading cell of 100 N. At least four replicate measurements were taken and averaged.

2.5. In vitro biological properties

2.5.1. Measurement of protein adsorption by surface plasmon resonance

The quantitative adsorption of HSA and HFb onto the polyurethane surfaces was studied by surface plasmon resonance (SPR), a unique surface sensing technique that allows realtime monitoring of different surface molecular interactions with very high sensitivity without the need for labels [28]. The interaction between HSA and HFb with SPEUU was studied by means of a home-made SPR biosensor developed in the authors' laboratory. The SPR sensor was established based on the Kretschmann configuration [29]. The Kretschmann configuration typically used in SPR instruments depends on a prism to measure SPR angles. In this configuration, incident light hits the gold layer on the opposite side of the immobilized biomolecules, posing strict requirements for the optical properties of the support substrate and the gold layer thickness. In the grating-coupled configuration, a fine grating on the chip surface provides optical coupling and allows imaging of the entire surface at once, enabling simultaneous realtime binding analysis at every spot on the surface. Here, incident light hits the gold layer from the top and through the biomolecular layer, avoiding the stringent need for an optical quality support substrate and specific gold layer thickness. Scheme 1 shows the SPR apparatus used in this work.

The sensor chip was a glass coverslip substrate on which a 65-nm-thick Au film was deposited by vacuum sputtering technology (Balzer PLS 500). Radiation from a He–Ne laser (632.8 nm) was modulated by a chopper and coupled to the system via a PMMA prism ($n = 1.405$). The reflected beam was then focused onto a photodiode detector, and the SPR signal was collected as a function of the measured incidence angle. For protein adsorption measurements, the Au slide was spin-coated with films from SPEUU solutions in DMAc (1 mg ml^{-1}). The coated slide was coupled to the prism with silicon as index matching fluid, and the fluid cell was mounted on the surface. The PBS was then driven into

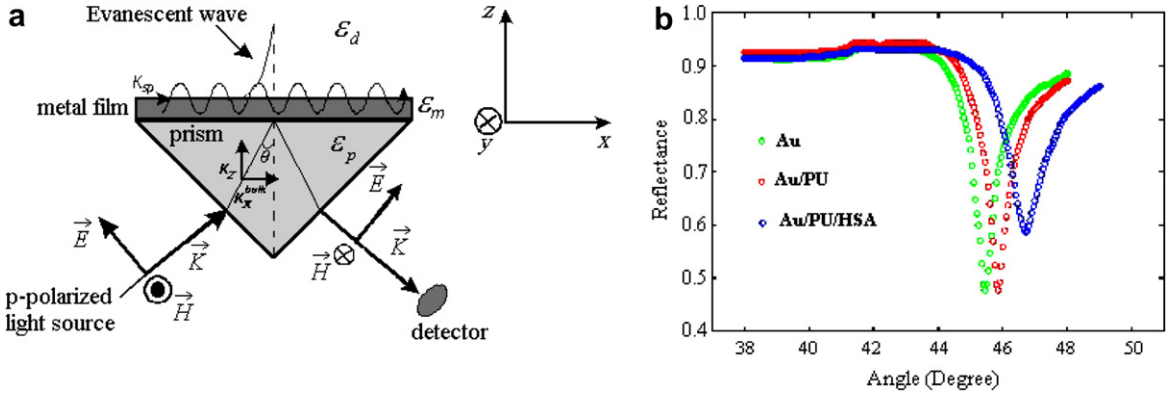

Scheme 1. (a) The Kretschmann configuration of the SPR apparatus used in this work, and (b) SPR spectra of PHL films after contact with human serum albumin (HSA) (4.2 mg L^{-1}) at 37 °C (experimental curves showed as an example of this method).

the cell to produce a physiological pH environment for protein adsorption, and the resonance angle A_1 was detected with the SPR software. The protein solution flowed into the fluid cell at a rate of 100 μl min^{-1}, and the SPR curve was monitored every 2 min until resonance angle remained unchanged. PBS was pumped into the cell again after 10 min to wash the proteins which did not bind tightly to the material surface, and the resonance angle A_2 was obtained. At least five measurements were performed for each protein. The amount of adsorbed proteins could be calculated from the resonance angle shift according to the relation $c = k\ (A_2–A_1)$, where c is the concentration of proteins adsorbed on material surfaces, and k is the weight of proteins per unit area and per unit degree. The sensitivity of SPR measurements was 1 ng mm^{-2} of adsorbed protein with the accession in SPR angle shift for 0.1°. Thus, the k value was 10 ng mm^{-2} deg^{-1}.

2.5.2. CD62P expression

In vitro platelet adhesion experiments were conducted to examine the interaction of blood with SPEUU-coated and uncoated ELISA plates. Platelet-rich plasma (PRP) was prepared from fresh blood drawn from healthy adult donors who had not taken aspirin-containing drugs for at least 10 days prior to donation. Blood was collected from antecubital veins into siliconized tubes containing citrate phosphate dextrose anticoagulant (0.7 mM citric acid, 9.3 mM sodium citrate and 13.6 mM dextrose) and adenine (CPD-A1, Sigma Co.) at a ratio of 1.4 and centrifuged at 800*g* for 10 min at 22 °C to obtain PRP. A volume of 200 μl was pipetted into a SPEUU-coated plate and incubated at 37 °C for 1 h. Immediately after incubation, 100 μl of PRP was put into tubes containing 20 μl of fluorescein isothiocyanate (FITC) conjugated anti-CD63 monoclonal antibody and the same amount of phycoerythrin (PE) conjugated anti-CD62P monoclonal antibody (Immunotech S.A.) and incubated at 25 °C. Then, the platelets were washed twice in PBS, and the number of antigen expressing platelets and the fluorescence intensity were measured with a flow cytometer. A group of platelets was gated, and the expressions and the fluorescence intensities of FITC and PE were measured at 525 nm and 575 nm, respectively. The ELISA assay detection limit for CD62P in this work was 1.05 ng L^{-1}.

2.5.3. Platelet adhesion

The SPEUU-coated and uncoated ELISA surfaces were incubated in the previously prepared PRP (200 μl) for 30 min at 37 °C. After washing in PBS, platelets were fixed by glutaraldehyde (1.5% solution in PBS) at room temperature. After addition of 10 μl of acridine orange, the epifluorescence of the labeled platelets was detected using a digital camera (Nikon Co.) mounted on an inverted microscope. A vapor mercury lamp filtered within the range 450–490 nm was used as excitation light. A long-pass filter allowed the fluorescence signal to be detected for wavelengths longer than 515 nm. The morphology of adhered platelets onto SPEUU films was observed by scanning electron microscopy (SEM) (JEOL XL30).

2.5.4. Kinetics of thrombus formation

The whole human blood was added to one part of acid–citrate–dextrose (ACD) for nine parts of blood. The resultant ACD blood was placed on a glass plate, PHH and PHL. Clotting was initiated by adding aqueous $CaCl_2$ solution, and the thrombus formed during 30 min was weighed. The relative weights of thrombus formed on different samples were determined, taking as reference the 100% of thrombus formed on a glass plate.

2.5.5. Cytotoxicity

A cytotoxicity assay was performed by adding dilutions of SPEUU extracts to a CHO cell culture on a Petri plate (15×60 mm^2). The positive and negative controls were a 0.02 vol.% phenol solution and ultra-high molecular-weight polyethylene (UHMWPE) [30], respectively.

Preparation of extracts. PHL, PHH and UHMWPE films (6 cm^2) were sterilized by gamma radiation (25 kGy) and poured into 100 ml glass flasks. Sixty milliliters of the culture medium MEM-FBS (minimum eagle medium with 10 vol.% fetal bovine serum and 1 vol.% penicillin and streptomycin solution) was added and incubated for 48 h at 37 °C. The supernatant was then filtered through a Millipore® membrane with 0.22 mm pores, and serial dilutions were made of the SPEUU, UHMWPE and 0.02 vol.% phenol solution (100, 50, 25, 12.5 and 6.25 vol.%) extracts. UHMWPE and phenol solution were used as negative and positive control, respectively.

Preparation of the primary culture. The CHO cells were cultivated in plastic bottles in a MEM-FBS medium, placed in an incubator at 37 °C with a humid atmosphere of 5 vol.% CO_2, until a cell layer was obtained. The culture medium was then removed from the incubator, and the cells were washed with calcium-free and magnesium-free phosphate-buffered saline solution (CMF-PBS). A 0.2 wt.% tripsine solution was added to detach the cells from the bottle. The cells were washed twice with CMF-PBS, re-suspended in MEM-FBS, and the suspension was finally adjusted to 100 cells ml^{-1}.

Cytotoxicity testing. From the above suspension, 2 ml was distributed on each culture plate (15×60 mm^2) and incubated for 5 h for cell adhesion. After this period, the culture medium was removed, and 5 ml of the pure extract and 5 ml of each serial dilution (50, 25, 12.5 and 6.25 vol.%) were added to the same plates. Fresh medium (MEM-FBS, 5 ml) was then placed on the plate of the CHO cell control. Each concentration of the tested extracts was made in triplicate. The plates were incubated in a humid incubator with 5 vol.% CO_2 at 37 °C for 7 days, after which the medium was removed and the colonies mixed with a solution of 10 vol.% formaldehyde diluted in a 0.9 wt.% saline solution and stained with Giemsa. The visible colonies on each plate were counted and compared with the number of colonies of the CHO cell control

plate. The cytotoxic potential of the material was expressed by an index of cytotoxicity, IC_{50} (%), which represents the concentration of the extract that suppresses the formation of cell colonies by 50% in comparison with the control.

3. Results and discussion

3.1. Macrodiol characterization

In order to obtain polymers with high molecular weight in linear polymerization, monomer concentrations must be adjusted. For this reason, great care was taken to determine the molecular weight of the macrodiol as accurately as possible before starting the synthesis of the polyurethanes [5]. ^{1}H NMR afforded structural information on PCL diol. The analysis confirmed that oligomers were constituted by TEG + CL units, and the ratio of CL to TEG signals afforded the value of Mn. Following the same analysis previously reported [5], the PCL spectrum revealed the presence of two different types of TEG units: monosubstituted TEG species (HO–TEG–PCL–OH, 9.58%) and disubstituted TEG species (HO–PCL–TEG–PCL–OH, 90.42%). No free TEG species were found. The Mn determined by end-group titration was more accurate than that estimated by NMR measurements: 2250 and 2490, respectively. The first was used for SPEUU formulations. FTIR showed the typical signals of aliphatic polyester: 3535 cm^{-1}, 2945 cm^{-1}, 2866 cm^{-1}, 1723 cm^{-1}, 1246 cm^{-1} and 1194 cm^{-1}.

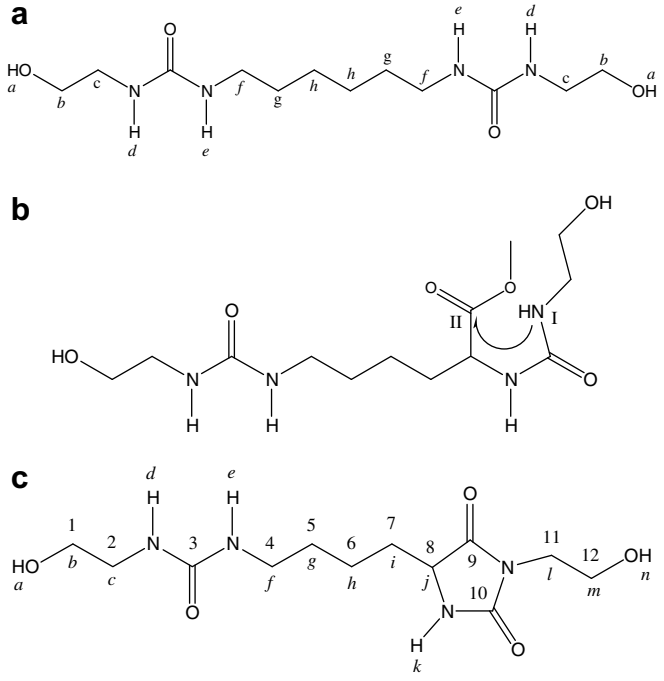

Scheme 2. Chemical structures of synthesized urea–diol chain extenders: (a) AE–H–AE; (b) intermediate of AE–L–AE formation; and (c) AE–L–AE, showing the proton (letters) and carbon (numbers) NMR assignments.

The glass transition temperature (T_g) and melting temperature (T_m) of PCL diol were observed at −69.3 °C and 50.5 °C, respectively. The degree of crystallinity of PCL diol was calculated taking into account the melting heat of PCL (96.9 J g^{-1}) and the crystallization heat for pure high molecular weight PCL (148.05 J g^{-1}) [31]. A crystallinity value of 65.5% was found.

3.2. Chain extenders synthesis and characterization

The chemical structure of the synthesized urea–diol chain extenders was determined by NMR and FTIR spectroscopy, and is shown in Scheme 2. The ^{1}H NMR spectrum of AE–H–AE is shown in Fig. 1a. The ratio of the area of peaks *d* and *e* to that of peak *a* (hydroxyl hydrogen) was 1.98:1, which confirms that the reaction of the amine groups of AE with HDI without catalyst forms a linear and symmetrical structure with two urea groups (Scheme

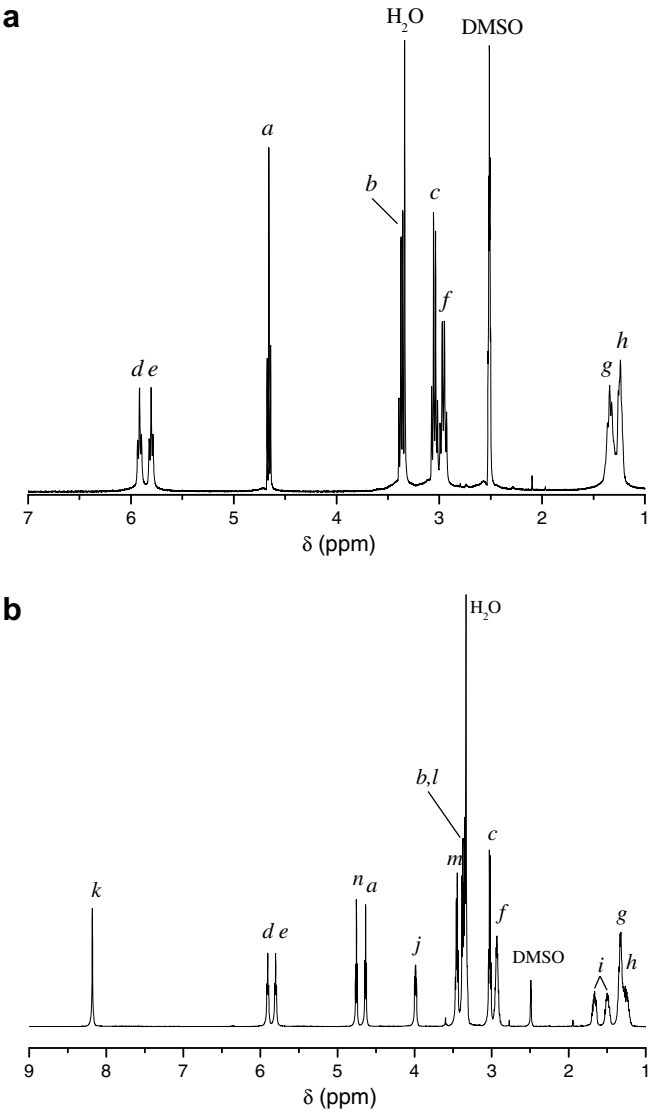

Fig. 1. ^{1}H NMR spectra of (a) AE–H–AE and (b) AE–L–AE chain extenders.

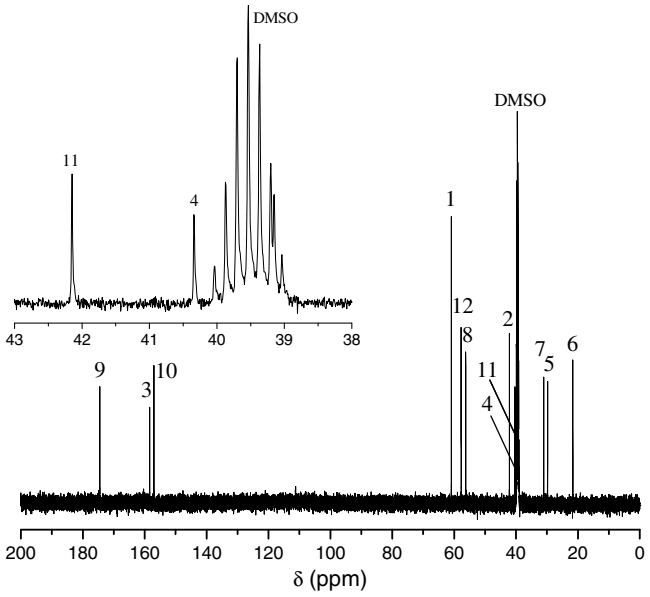

Fig. 2. ^{13}C NMR spectrum of AE–L–AE chain extender.

2a). The analysis of the ^{1}H NMR spectrum of AE–L–AE (Fig. 1b) turned out to be more difficult than the one performed for AE–H–AE. The signal assignments, peak area and chemical shifts did not correspond to the structure of the expected product, a diurea–diol (Scheme 2b). Therefore, the chemical structure of the obtained compound was elucidated by means of ^{13}C NMR (Fig. 2) and ^{1}H ^{13}C NMR heteronuclear single quantum correlation (HSQC) (data not shown). The analysis of these spectra revealed the structure of AE–L–AE (Scheme 2c). Owing to the presence of a methyl-ester short-chain branch in LDI, AE–L–AE has a different structure. First, the amine groups of AE reacted with LDI to produce the diurea shown in Scheme 2b. Then, a reaction of intramolecular aminolysis between the nucleophilic nitrogen (I) and the carbonyl carbon (II) led to the formation of the final product, a five-membered ring structure of 1,3-imidazolidine-2,4-dione (hydantoin). Thus, AE–L–AE presents an asymmetric hydroxyl-terminated structure composed of only one urea group and a heterocyclic-planar 3,5-disubstituted hydantoin.

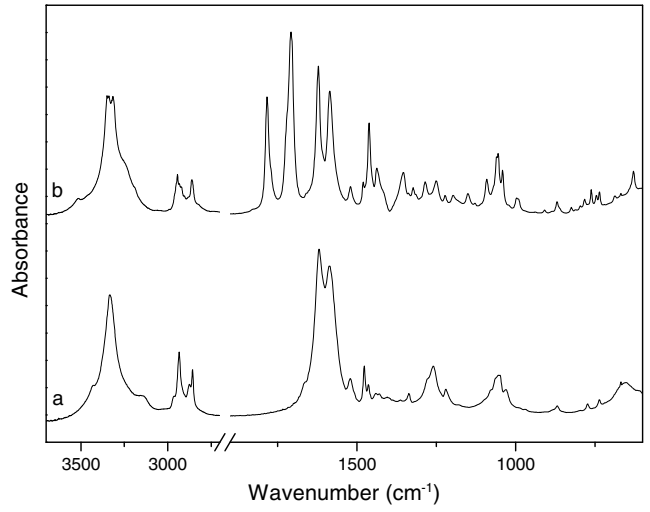

Fig. 3. FTIR spectra of chain extenders: (a) AE–H–AE and (b) AE–L–AE.

FTIR spectra of both chain extenders are shown in Fig. 3. The absence of the peak at 2250–2280 cm^{-1} corresponding to the isocyanate group indicates that the reaction was completed. The amine region of the AE–H–AE spectrum displayed a broad peak centered at 3332 cm^{-1}, which corresponds to N–H stretching in hydrogen-bonded urea groups. No evidence of any free N–H groups was observed (3515 cm^{-1}). This is related to the high symmetry of the chemical structure and the presence of an even number of carbon atoms in the chain extender, which allowed a close chain association. In the carbonyl region, the strong bands at 1619 and 1588 cm^{-1} were attributed to hydrogen-bonded carbonyl–urea amide I groups and urea amide II groups (C–N stretching and N–H bending). In the amine region of the AE–L–AE spectrum, not only did the signal of hydrogen-bonded N–H groups appear, but also another peak at 3515 cm^{-1}, corresponding to free N–H groups. This fact can be attributed to the asymmetric and cyclic structure of the chain extender, which inhibited the complete association of N–H groups by hydrogen bonding. In the carbonyl region, the strong bands at 1784 and 1708 cm^{-1} were attributed to carbonyl groups of the hydantoin cycle; the bands at 1622 and 1586 cm^{-1} were ascribed to hydrogen-bonded carbonyl–urea amide I groups and urea amide II groups, as in the case of AE–H–AE. As expected, the vibration corresponding to carbonyl ester in LDI (1743 cm^{-1}) was not observed.

The thermal analysis showed the crystalline nature of both chain extenders. DSC thermograms of AE–H–AE displayed a single endotherm, with a peak at 193.6 °C, and a melting heat of 210 J g^{-1}. The presence of two urea linkages and high structural symmetry led to a crystalline compound with high melting temperature. The thermal behavior of AE–L–AE was quite similar, exhibiting an endothermic peak at lower temperature (118.8 °C) and lower melting heat (150 J g^{-1}). This is consistent with the presence of only one urea group by molecule. Both urea–diol compounds evidenced good solubility in water, DMAc and DMSO.

3.3. SPEUU synthesis and characterization

Two aliphatic SPEUU based on PCL soft segments and hard segments of HDI extended with either AE–L–AE or AE–H–AE urea–diol were synthesized. PHL and PHH had approximately the same hard segment content, 22.2% and 21.8%, respectively. The polymers obtained were non-sticky, clear and slightly whitish. The synthetic pathway is detailed in Scheme 3. At the first stage, PCL diol was end-capped with HDI to form the macrodiisocyanate. At the second stage, the chain extender was added to

(a) Chemical structure of the synthesized PCL diol

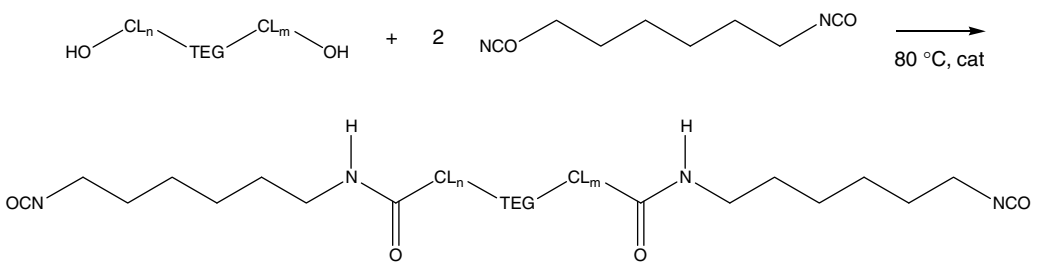

(b) Synthesis of isocyanate-endcapped PCL prepolymer

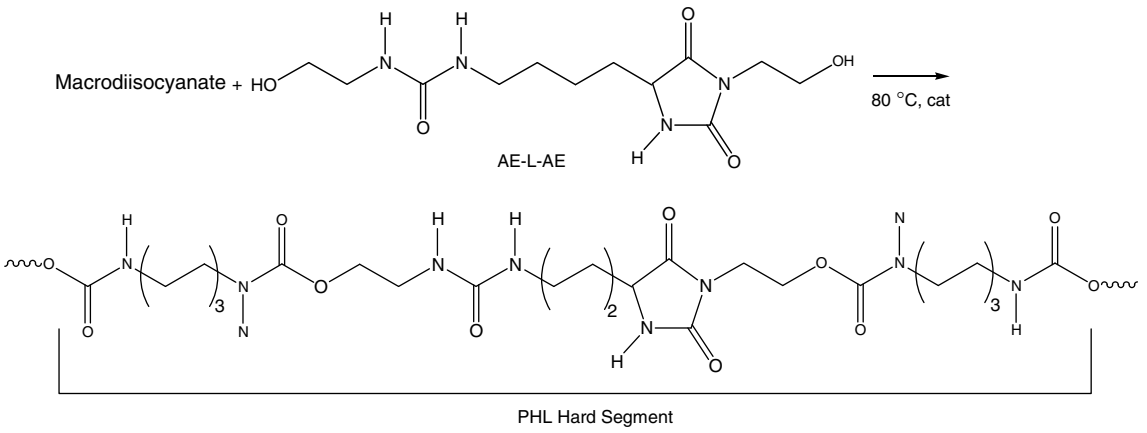

(c) Synthesis of SPEUU based on AE-L-AE chain extender

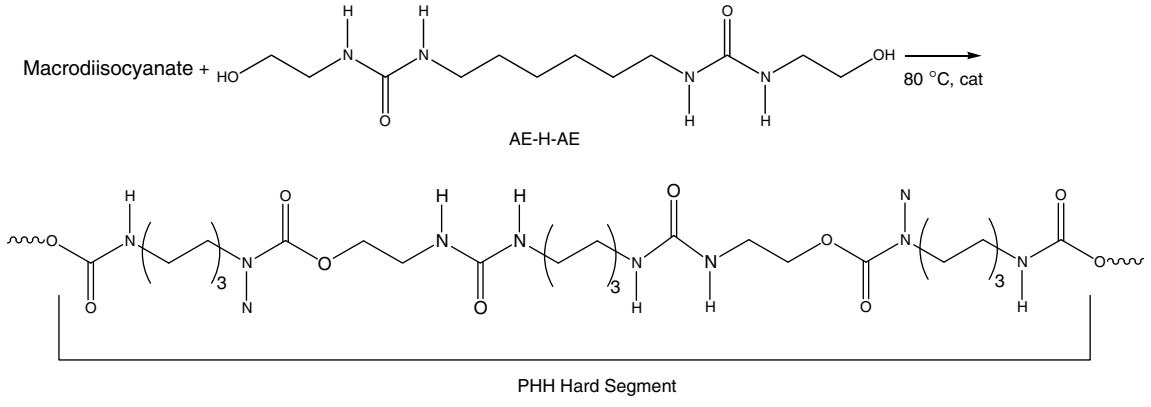

(d) Synthesis of SPEUU based on AE-H-AE chain extender

Scheme 3. Synthetic pathway followed for SPEUU preparation.

increase the molecular weight. After 6 h, complete disappearance of the isocyanate groups was observed by FTIR. In the case of PHH, the strong absorption of ester groups appeared at 1724 cm^{-1}, and its shoulder peak at a lower wavelength (1685 cm^{-1}) was attributable to carbonyl–urethane amide I groups (Fig. 4), demonstrating the formation of urethane groups which connect soft to hard segments. For PHL, the shoulder of the 1724 cm^{-1} peak appeared at 1680 cm^{-1}, close to the carbonyl band of the hydantoin group located at 1704 cm^{-1}.

SPEUU thermal properties were analyzed by DSC and are summarized in Table 1. For PHL, the first scan showed

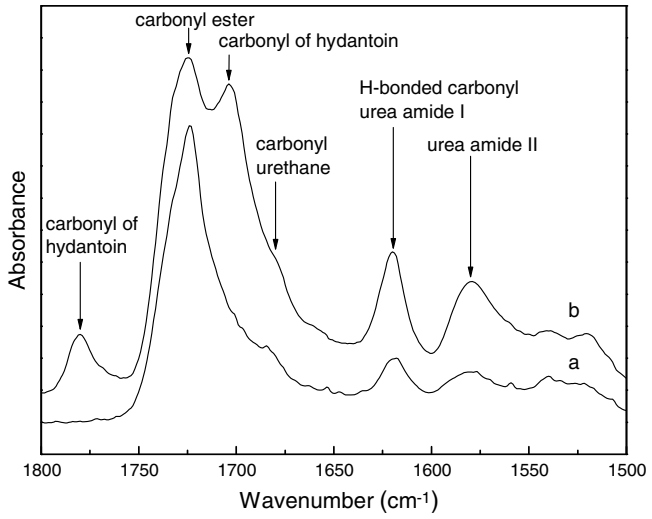

Fig. 4. Carbonyl region of the ATR-FTIR spectra: (a) PHH and (b) PHL.

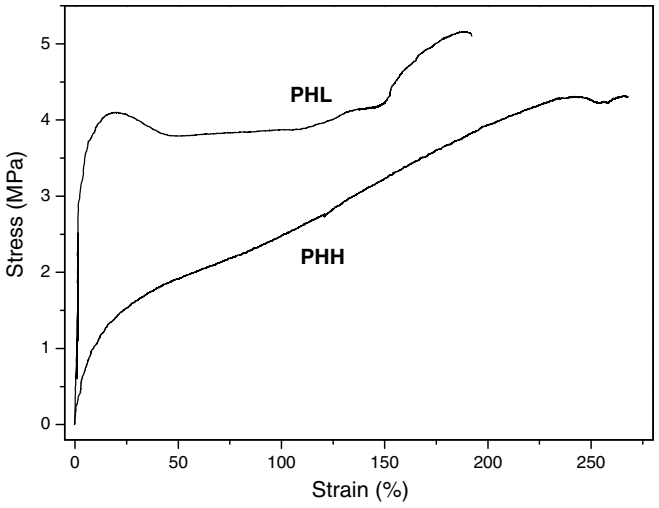

Fig. 5. Tensile stress–strain curves of PHL and PHH.

a T_g of soft segments ($T_{g,s}$) at −61.1 °C, indicating a certain degree of phase-mixed morphology. The soft segment melting endotherm ($T_{m,s}$) was observed at 44.4 °C, a temperature above body temperature and close to the reported values for other biomedical SPEUU [2,17]. The crystallinity of PCL in PHL was 30.4%, lower than that noted for pure PCL (65.5%). No glass transition temperature of hard domains ($T_{g,h}$) was observed. However, an endothermic peak attributable to the melting of hard segments appeared at 101.1 °C. After quenching from 110 °C to −150 °C, the second scan exhibited a lower $T_{g,s}$, an exotherm peak at −28.6 °C corresponding to the PCL crystallization, and a melting endotherm peak at 40.2 °C. No transitions attributable to hard segments were observed in the second scan.

As expected, the thermal transitions of PHH soft segments were close to those observed for PHL (Table 1). At high temperatures, a second-order transition appeared at 108.2 °C. This transition was not seen in PHL, and it was ascribed to $T_{g,h}$. A small exotherm was observed at 130.6 °C followed by an endotherm at 162.2 °C. These transitions can be attributed to hard segment crystallization and melting of crystalline hard domains, respectively. It is evident that the structural symmetry and presence of two urea linkages in PHH led to hard segment association and hard domain formation, which contributed to enhancing the phase separation. After quenching from 110 °C to −150 °C, the second scan exhibited soft-segment transitions similar to those observed for PHL. However, hard segment transitions in PHH were still observed, the $T_{g,h}$, $T_{c,h}$ and $T_{m,h}$ values being lower than those displayed in the first scan. The results of the thermal properties are in good agreement with the reported ones for other polyurethanes, some of which were intended for cardiovascular applications.

The intrinsic viscosity values of PHL and PHH samples were similar, 0.406 and 0.402 dl g^{-1}, respectively. These values indicate that the chain extender structure did not affect the molecular weight of the polymer.

Stress–strain curves for PHL and PHH samples are shown in Fig. 5. Polyurethanes exhibited a clearly different mechanical behavior. PHL displayed a pronounced yield point (~4.1 MPa at 19% strain) followed by necking and cold-drawing. In contrast, PHH behaved as a soft elastic material, showing a smooth transition in stress–strain behavior from the elastic to plastic deformation regions similar to crosslinked rubbers. It is evident that the symmetry and chemical structure of the AE–H–AE chain extender increased the ability of the hard segment to act as a physical crosslinking site. PHL displayed a higher Young's modulus than PHH, the mean values being 69.5 and 14.5 MPa, respectively. However, both polyurethanes exhibited similar toughness.

3.4. In vitro biological properties

3.4.1. Protein adsorption

Despite the extensive literature in the field, the biological basis of the biomaterial/blood interactions is still

Table 1
Thermal properties of SPEUU determined by DSC measurements

SPUU	$T_{g,s}$ (°C)	$T_{c,s}$ (°C)	$\Delta H_{c,s}$ (J g^{-1})	$T_{m,s}$ (°C)	$\Delta H_{m,s}$ (J g^{-1})	X_c (%)	$T_{g,h}$ (°C)	$T_{c,h}$ (°C)	$\Delta H_{c,h}$(J g^{-1})	$T_{m,h}$ (°C)	$\Delta H_{m,h}$ (J g^{-1})
PHL	–61.1	–	–	44.4	35.0	30.4	–	–	–	101.1	6.4
PHL-q[a]	–62.7	–28.6	39.1	40.2	49.9	9.4	–	–	–	–	–
PHH	−61.4	–	–	39.9	31.5	27.2	108.2	130.6	0.7	162.2	3.4
PHH-q[a]	−63.5	−34.3	16.0	40.6	34.5	16.0	98.2	124.1	2.3	152.0	2.7

[a] After quenching from 110 °C.

uncertain, as the adverse events that are initiated when the material is exposed to blood are numerous and complex [32,33]. It is generally believed that, when a synthetic material is exposed to blood, the first event that takes place is the adsorption of proteins onto its surface, followed by platelet adhesion and activation. HSA and HFb adsorption onto PHL and PHH were studied with the purpose of examining the extent of the surface interaction with proteins in physiological solution. From the SPR angle shift and a calibration curve of protein concentration, the amount of HSA and HFb adsorbed on PHH and PHL surfaces was calculated as a function of time (Fig. 6). Results show that the amount of HSA adsorbed on PHH films was higher than on PHL films. The increased HSA adsorption onto PHH can be ascribed to the presence of hydrophobic PCL domains on the SPEUU surface. This is consistent with the observation of a more pronounced phase separation in PHH compared with PHL. However, the analysis of microheterogeneous surfaces that exhibit microdomain structures with hydrophobic and hydrophilic regions, different surface charges and microcrystallinity made it complex to elucidate the factors that determine the observed behavior. It is well known that the type and amount of blood proteins adsorbed at the biomaterial/blood interface largely dictate the surface-induced platelet activation. In this sense, the adsorption of fibrinogen is known to accelerate platelet adhesion and activation. However, albumin adsorption on the synthetic surfaces can inhibit platelet activation and, therefore, does not promote clot formation. The large HSA adsorption onto both PHH and PHL films and the lower HFb adsorption may be a good indication of low platelet adhesion and activation by these surfaces.

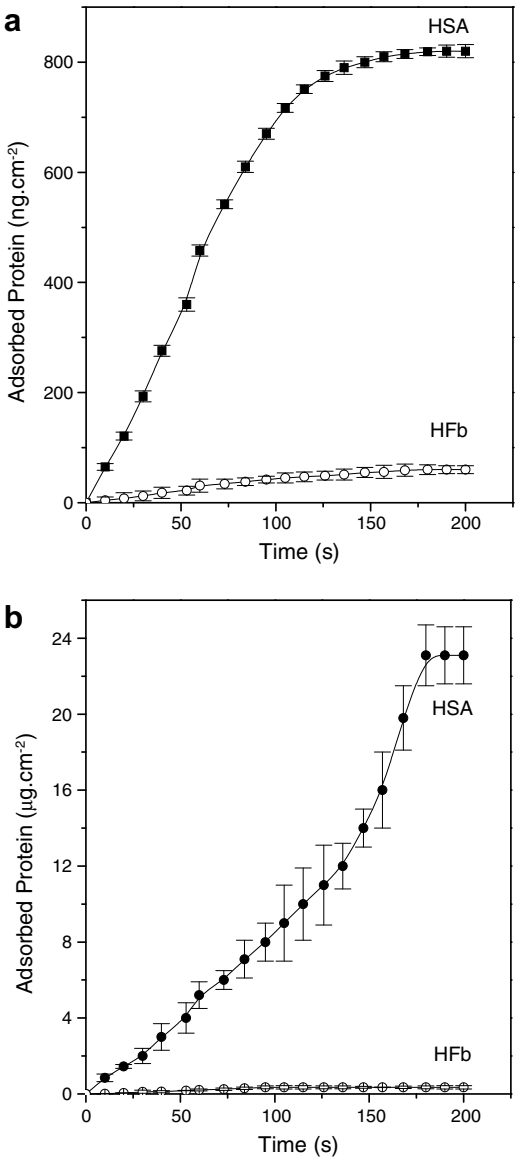

Fig. 6. Albumin (HSA) and fibrinogen (HFb) adsorption onto (a) PHL, and (b) PHH films measured by SPR technique at 37 °C.

3.4.2. Platelet adhesion, CD62P expression, kinetics of thrombus formation and cytotoxicity

Platelets play a key role in biomaterial-associated thrombosis, and a reduction in platelet adhesion and activation is vital for the eventual success of numerous blood-contacting medical applications. In this study, platelet adhesion in PHH and PHL was investigated, and the behavior of human platelets onto the SPEUU surfaces was examined by SEM. Epifluorescence micrographs of PHL- or PHH-coated ELISA plates and uncoated ELISA plates after incubation with human blood for 15 min at 37 °C are shown in Fig. 7. The uncoated ELISA surfaces appear to encourage platelet adhesion and activation with thrombus formation, whereas the PHH- and PHL-coated ELISA surfaces were essentially free from both platelet adhesion and thrombus formation. Platelet activation produces a cytoskeletal reorganization that results in characteristic cell shape changes: platelets lose their discoid shape and begin to develop thin pseudopodia. It is well known from haemostasia studies that, at more advanced stages, they become large, spiny spheres completely covered by pseudopodia, and finally become fully spread. In this study, the number of adherent platelets and the platelet-covered area were determined as markers of surface thrombogenicity, using SEM analysis. Both the number of platelets and the changes in morphological shape in active platelets contribute to the platelet-covered surface area of the substrate. Thus, calculating the platelet-covered area per unit area provides an index that reflects platelet adhesion and activation. The ratio of platelets per unit area adhered to the surfaces of substrates coated with PHH and PHL films after incubation is displayed in Fig. 8. Glass and medical-grade silicone (mgSi) were used as positive and negative controls, respectively. The proportions of platelet-covered area for PHH and PHL were not significantly higher than that for silicone substrates. Fig. 9 shows SEM micrographs of PHH and PHL coatings as well as the uncoated ELISA plate as positive control after contact with human blood. Platelet activation was markedly suppressed with the PHH or PHL coatings (Fig. 9c and d),

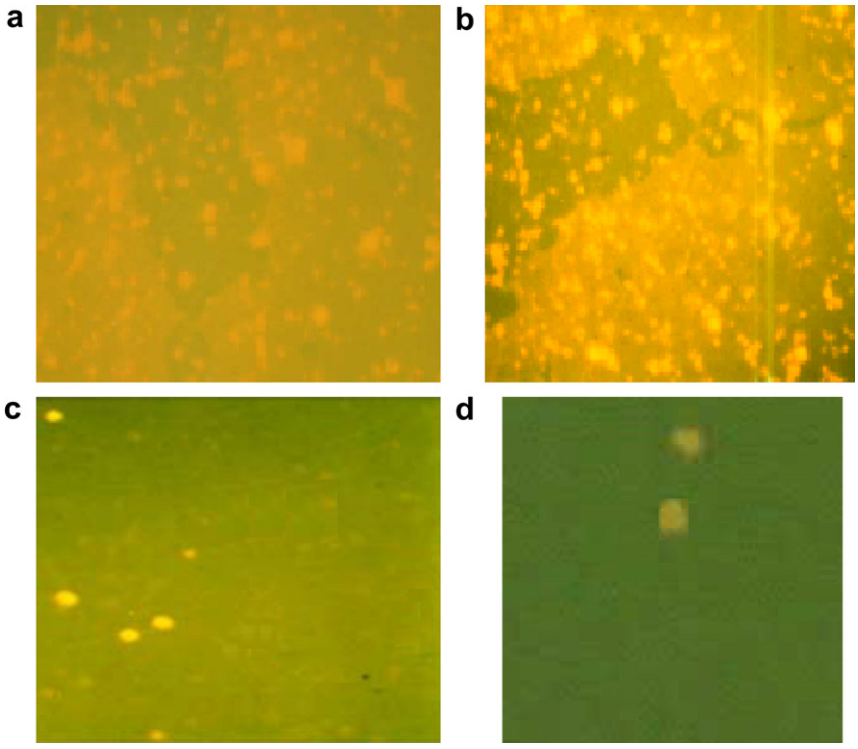

Fig. 7. Representative epifluorescence microscopy images of platelets on uncoated ELISA plates (a, b) and coated ELISA plates with PHL (c) and PHH (d) after blood exposition (×1000).

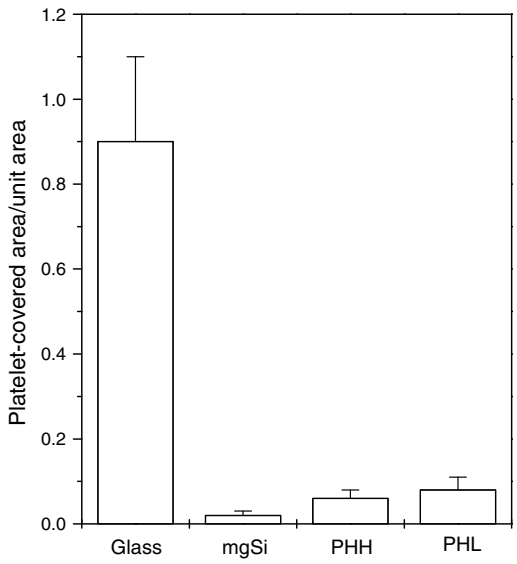

Fig. 8. Ratio of platelet-covered area per unit area (100,000 μm^2) on the surfaces of substrates coated with PHH and PHL films after 60 min incubation with human PRP.

and this can be ascribed to the high HSA adsorption by these surfaces.

In biological conditions, platelets circulate in a quiescent state without interacting with each other or with other cells in the vascular system, such as leukocytes or endothelial cells. Upon activation with a wide range of agonists, platelets rapidly expose receptors/molecules to support adhesion, spreading and aggregation at vascular damaged sites. Both platelets and endothelial cells have been reported to mobilize the surface adhesion of the molecule P-selectin (CD62 P) from intracellular granule stores within minutes following activation with agonists such as thrombin. The CD62P antigen, also known as platelet activation-dependent granule-external membrane protein, is a 140 kDa single-chain polypeptide. Previous studies have shown that CD62P antigen is secreted on the platelet–membrane surface when the platelet is activated by external stimulation such as contact with synthetic surfaces. [34] Fig. 10 shows the results in percentages of CD62P positive cells. From a material standpoint, a significant difference was observed in the proportion of CD62P expressing platelets on the PHH or PHL coatings compared with the uncoated ELISA plates. It is evident that the uncoated ELISA plates show higher platelet adhesion, in accordance with the epifluorescence results.

The kinetics of thrombus formation after exposure of the SPEUU coatings to human blood is shown in Fig. 11. The thrombus formation decreased drastically with the PHH and PHL coatings, in accordance with the HSA adsorption results. The lower HFb adsorption appeared to delay the contact activation of intrinsic coagulation (Fig. 6). Finally, the cytotoxicity level of SPEUU samples was relatively low (Fig. 12), and it might be well worth performing further studies of these materials using animal models in order to gain insight into the material behavior within the biological media. Based on the results obtained and focusing on the application of the synthesized SPEUU in the tissue-engineering field, degradation behavior and

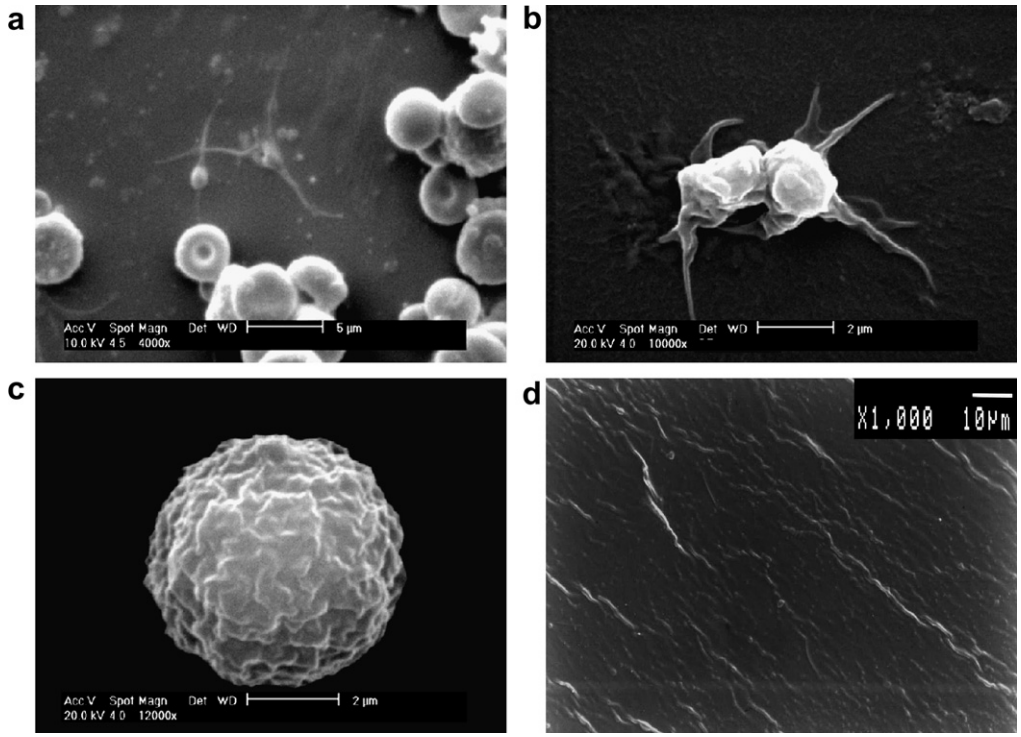

Fig. 9. SEM micrographs of PHH and PHL surfaces after incubation with human blood at 37 °C for 15 min. (a, b) Uncoated ELISA plates; illustration of non-activated blood platelet onto (c) PHH and (d) PHL coatings.

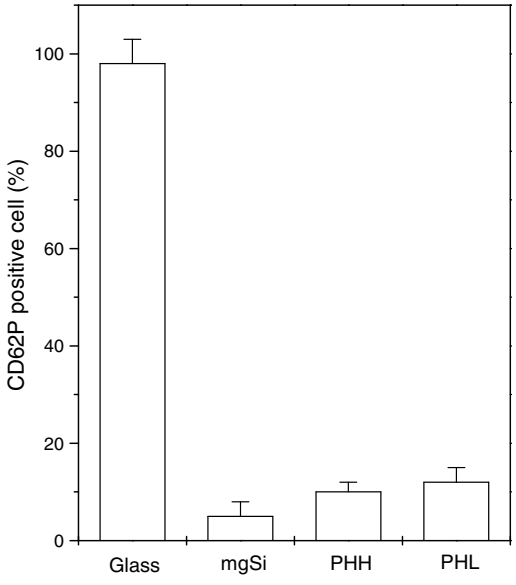

Fig. 10. Expression of CD62P positive platelets (%). The Pearson (P) correlation is 0.025.

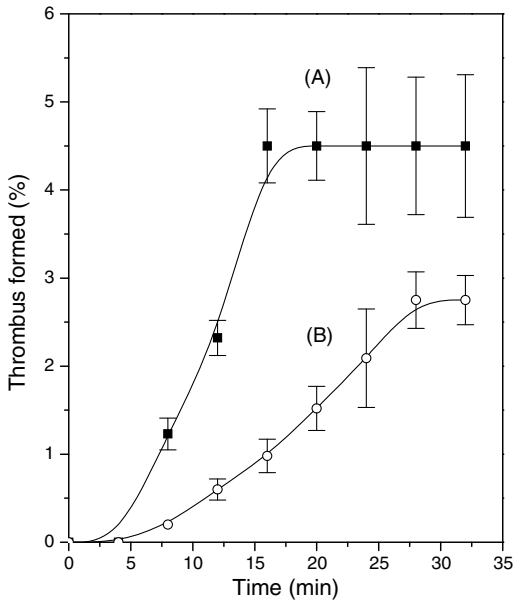

Fig. 11. Kinetics of thrombus formation on (A) PHL, and (B) PHH.

processing into scaffolding materials are currently being investigated.

4. Conclusion

Two aliphatic segmented poly(esterurethane urea)s were successfully synthesized using urea–diol chain extenders. The different chemical structure of chain extenders modulated the phase separation of soft and hard segments, as demonstrated by the thermal behavior. Hard segment association was enhanced using a symmetric diurea–diol chain extender. The resultant morphology had an important effect on the mechanical properties. The higher albumin and lower fibrinogen adsorption in both SPEUU samples, as well as the suppression of platelet activation and cytocompatibility, indicated that these SPEUU are

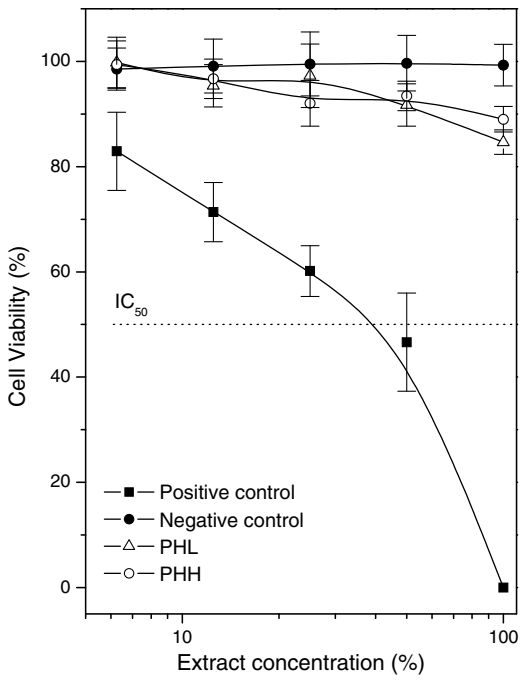

Fig. 12. Cytotoxicity of the SPEUU extracts, negative control (UHMWPE), and positive control (phenol) against Chinese hamster ovary (CHO) cells.

promising biomaterials for tissue engineering applications. Studies of biodegradation behavior and scaffold preparation are being carried out, and the results will be reported elsewhere.

Acknowledgements

The authors would like to thank ANPCyT and CONICET (Argentina), CNPq and Capes (Brazil) for financial support. The donation of LDI by Kyowa Hakko (Japan) is gratefully acknowledged.

References

[1] Mathur AB, Collier TO, Kao WJ, Wiggins M, Schubert MA, Hiltner A, et al. In vivo biocompatibility and biostability of modified polyurethanes. J Biomed Mater Res 1997;36:246–57.
[2] Gorna K, Gogolewski S. Novel biodegradable polyurethanes for medical applications. In: Agrawal CM, Parr JE, Lin ST, editors. Synthetic bioabsorbable polymers for implants. ASTM STP 1396. West Conshohocken (PA): American Society for Testing and Materials; 2000. p. 39–57.
[3] Gunatillake PA, Adhikari R. Biodegradable synthetic polymers for tissue engineering. Euro Cell Mater 2003;5:1–16.
[4] Bruin P, Veenstra GJ, Nijenhuis AJ, Pennings AJ. Design and synthesis of biodegradable poly(ester–urethane) elastomer networks composed of non-toxic building blocks. Macromol Chem, Rapid Commun 1988;9:589–94.
[5] Marcos-Fernández A, Abraham GA, Valentín JL, San Román J. Synthesis and characterization of biodegradable non-toxic poly(ester–urethane–urea)s based on poly(ε-caprolactone) and amino acid derivatives. Polymer 2006;47:785–98.
[6] Lelah MD, Cooper SL. Polyurethanes in medicine. Boca Raton (FL): CRC Press; 1987.
[7] Estes GM, Cooper SL, Tobolsky AV. J Macromol Sci Rev Macromol Chem 1970;C4(2):313–66.
[8] Shi FY, Wang LF, Tashev E, Leong KW. Synthesis and characterization of hydrolitically labile poly(phosphoester–rethanes). In: Dunn RL, Ottenbrite RM, editors. Polymeric drugs and drug delivery systems. ACS symposium series 469. Washington (DC): American Chemical Society; 1991. p. 141–54.
[9] Skarka GA, Woodhouse KA. Synthesis and characterization of degradable polyurethane elastomers containing an amino acid-based chain extender. J Biomater Sci Polym Ed 1998;9:271–95.
[10] Guelcher SA et al. Synthesis of biocompatible segmented polyurethanes from aliphatic diisocyanates and diurea diol chain extenders. Acta Biomater 2005;1:471–84.
[11] Guan J, Sacks MS, Beckman EJ, Wagner WR. Synthesis, characterization, and cytocompatibility of elastomeric, biodegradable poly(ester–urethane)ureas based on poly(caprolactone) and putrescine. J Biomed Mater Res 2002;61:493–503.
[12] de Groot JH, de Vrijer R, Wildeboer BS, Spaans CJ, Pennings AJ. New biomedical polyurethane ureas with high tear strengths. Polym Bull 1997;38:211–8.
[13] Guan J, Fujimoto KL, Sacks MS, Wagner WR. Preparation and characterization of highly porous biodegradable polyurethane scaffolds for soft tissue applications. Biomaterials 2005;26:3961–71.
[14] Spaans CJ, de Groot JH, Dekens FG, Pennings AJ. High molecular weight polyurethanes and a polyurethane urea based on 1,4-butate-diisocyanate. Polym Bull 1998;41:131–8.
[15] Abraham GA, Marcos-Fernández A, San Román J. Bioreabsorbable poly(ester ether urethane)s from L-lysine diisocyanate and triblock copolymers with different hydrophilic character. J Biomed Mater Res 2006;76A:729–36.
[16] Skarja GA, Woodhouse KA. Structure–property relationships of degradable polyurethane elastomers containing an amino acid-based chain extender. J Appl Polym Sci 2000;75:1522–34.
[17] Skarja GA, Woodhouse KA. Synthesis and characterization of degradable polyurethane elastomers containing an amino acid-based chain extender. J Biomater Sci Polym Ed 1998;9:271–95.
[18] Heijkants RCJC et al. Design, synthesis and properties of a degradable polyurethane scaffold for meniscus regeneration. J Mater Sci Mater Med 2004;15:423–7.
[19] Heijkants RGJC et al. Uncatalyzed synthesis, thermal and mechanical properties of polyurethanes based on poly(ε-caprolactone) and 1,4-butane diisocyanate with uniform hard segment. Biomaterials 2005;26:4219–28.
[20] Gorna K, Gogolewski S. In vitro degradation of novel medical biodegradable aliphatic polyurethanes based on ε-caprolactone and pluronics with various hydrophilicities. Polym Deg Stab 2002;75:113–22.
[21] de Groot JH, de Vrijer R, Pennings AJ, Klompmaker J, Veth RPH, Jansen HWB. Use of porous polyurethanes for meniscal reconstruction and menical prostheses. Biomaterials 1996;17:163–73.
[22] Shau MD, Tseng SJ, Yang TF, Cherng JY, Chin WK. Effect of molecular weight on the transfection efficiency of novel polyurethane as a biodegradable gene vector. J Biomed Mater Res 2006;77A:736–46.
[23] Takahara A, Hadano M, Yamaguchi T, Otsuka H, Kidoaki S, Matsuda T. Characterization of novel diodegradable segmented polyurethanes prepared from amino-acid based diisocyanate. Macromol Symp 2005;224:207–17.
[24] Spaans CJ, de Groot JH, Belgraver VW, Pennings AJ. A new biomedical polyurethane with a high modulus based on 1,4-butane-diisocyanate and ε-caprolactone. J Mater Sci Mater Med 1998;9:675–8.
[25] Kavlock KD, Pechar TW, Hollinger JO, Guelcher SA, Goldstein AS. Synthesis and characterization of segmented poly(esterurethane urea) elastomers bor bone tissue engineering. Acta Biomater 2007;3:475–84.
[26] Basse Asplund JO, Bowden T, Mathisen T, Hilborn J. Variable hard segment length in poly(urethane urea) through excess of diisocyanate

and vapour phase addition of water. Macromolecules 2006;39:4380–5.
[27] Abraham GA, De Queiroz AA, San Roman J. Hydrophilic hybrid IPNs of segmented polyurethanes and copolymers of vinylpyrrolidone for applications in medicine. Biomaterials 2001;22:1971–85.
[28] Green RJ, Frazier RA, Shakeshe KM, Davies MC, Roberts CJ, Tendler SJB. Surface plasmon resonance analysis of dynamic biological interactions with biomaterials. Biomaterials 2000;21:1823–35.
[29] Homola J, Yee SS, Gauglitz G. Surface plasmon resonance sensors: review. Sens Actuators B 1999;54:3–15.
[30] ISO 10993-5. Biological evaluation for medical devices tests for cytotoxicity in vitro methods international standards organization. Geneva: ISO; 1999.
[31] Van Krevelen DW. Properties of polymers. Amsterdam: Elsevier; 1990, p. 121.
[32] Ratner BD. Blood compatibility—a perspective. J Biomater Sci Polym Ed 2000;11:1107–19.
[33] Brash JL. Exploiting the current paradigm of blood-material interactions for the rational design of blood-compatible materials. J Biomater Sci Polym Ed 2000;11:1135–46.
[34] Hamburger SA, McEver RP. GMP-140 mediates adhesion of stimulated platelets to neutrophils. Blood 1990;75:550–4.